TOWARDS EMPIRICISM-FREE LARGE EDDY SIMULATION FOR THERMO-HYDRAULIC PROBLEMS

V.M. Goloviznin[1], S.A. Karabasov[1,2], M.A. Zaitsev[1]
[1]Moscow Institute of Nuclear Safety, Russian Academy of Science, Moscow, Russia
[2]University of Cambridge Department of Engineering, Cambridge, UK

Abstract

A novel high-resolution Navier-Stokes method is proposed for modelling large-scale turbulent flows. The method is based on the non-oscillatory low-dissipative and low-dispersive CABARET scheme. Numerical results are provided for the classical backward-facing step problem and for the recent OECD/NEA-Vattenfall T-junction blind-test exercise.

1. Introduction

Unsteady heat transfer problems that are associated with turbulent non-isothermal flow mixing are very topical for the thermal fatigue of industrial power plant systems. Mathematical modelling of such problems remains very challenging because of the poorly understood large-scale turbulence phenomena. One popular approach for modelling this type of flows is Implicit Large Eddy Simulation (ILES). The Implicit LES approach doesn't have any explicit turbulence model and has to rely on (i) the ability of the numerical method to remove all scales smaller than the grid scale from the solution without affecting the resolved scales, in provision that (ii) the method's resolution is enough to capture all important dynamic scales. For the latter, the use of high-resolution robust numerical methods is thus essential. Hence, for the numerical method our choice is the Compact Accurately Boundary Adjusting High REsolution Technique (CABARET) scheme that has previously been applied for solving advection-dominated problems [1-6]. In comparison with the standard finite-difference and finite-volume methods, in CABARET there is always an additional independent evolutionary variable, which gives the method the ability to preserve one more important property of the governing equations - the small phase and amplitude error. For solving Navier-Stokes equations with Reynolds numbers of 10^4, the method gives a very good convergence without any additional preconditioning down to Mach numbers as low as M~0.05-0.1 In particular for the ILES modelling of a hydrodynamic instability and free jet a 257^2 grid using CABARET is able to produce results comparable to a conventional second-order method which would require at least 1025^2 grid points [6]. Here, the CABARET method is 30 times more efficient.

The goal of the current paper is to further promote the ILES CABARET method for modelling of large-scale turbulent flows. We first consider the solution of the benchmark problem of turbulent flow over a backward facing step [7] and then discuss the CABARAT application for the recent OECD/NEA-Vattenfall T-junction blind test exercise [8,9].

1. Turbulent flow over backward facing step: example of the solution for a classical benchmark problem

To first demonstrate the CABARET solver performance in idealised framework the flow over backward facing step [7] is considered. The step height S is the same as the gap between the step and the top wall boundary. The inflow boundary conditions are laminar, with Reynolds number=5000 and Mach number=0.1. Uniform hexahedral grids have been used with densities of 10 points and 20 points per the step height (S) giving a total grid size of 100 000 and 800 000 points, respectively. The CABARET solution was obtained from conducting a fully compressible Navier-Stokes calculation which technical details, including the parallelization strategies, are reported elsewhere, e.g., in [10], and here we are just reporting the results. Figure 1 shows numerical results: the time-averaged axial velocity component and velocity streamlines for two grid resolutions - (a) and a snapshot of instantaneous vorticity filaments - (b).

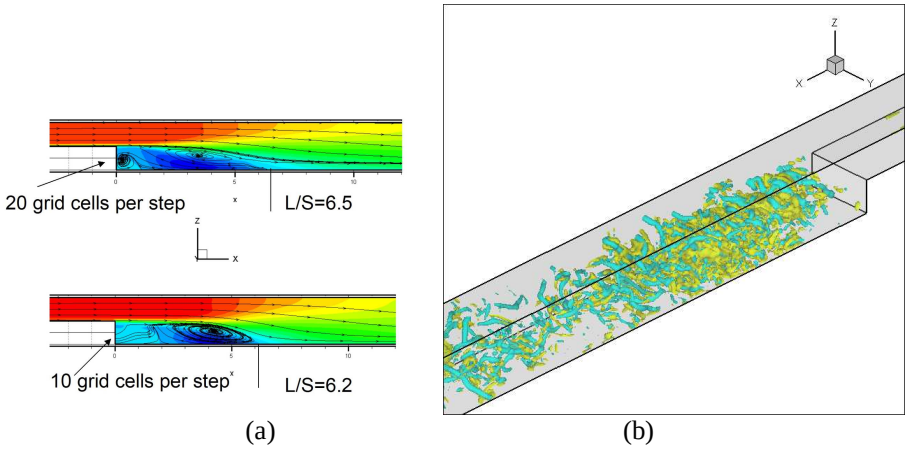

(a) (b)

Fig. 1. Time-averaged velocity fields for two mesh resolutions (a) and vorticity (Q-norm) iso-surfaces for the grid density of 20 cells per step (b).

The instantaneous vorticity field has a rich 3D structure typical of a high-Re turbulent flow and is in a drastic contrast with the 2D laminar shear-layer profile that has been used as the initial condition. We also note that the length of the recirculation zone after the step is in a good agreement with the reference experiment value range at this Reynolds number, L/S=6.5-7 [7].

2. The CABARET solution of the T-junction problem

2.1 Governing equations and boundary conditions

The modelling of thermo-hydraulic turbulent flow in the T-junction corresponding to the OECD/NEA-Vattenfall T-junction blind test conditions [8,9] is discussed next.

The water flow in mixing tees is modelled by the system of slightly compressible Navier-Stokes equations:

$$
\begin{aligned}
&\frac{\partial p}{\partial t}+\rho_0 c^2\left(\frac{\partial u}{\partial x}+\frac{\partial v}{\partial y}+\frac{\partial w}{\partial z}\right)=0\\
&\frac{\partial u}{\partial t}+u\frac{\partial u}{\partial x}+v\frac{\partial u}{\partial y}+w\frac{\partial u}{\partial z}=-\frac{1}{\rho_0}\frac{\partial p}{\partial x}+\upsilon\left(\frac{\partial^2 u}{\partial x^2}+\frac{\partial^2 u}{\partial y^2}+\frac{\partial^2 u}{\partial z^2}\right)\\
&\frac{\partial v}{\partial t}+u\frac{\partial v}{\partial x}+v\frac{\partial v}{\partial y}+w\frac{\partial v}{\partial z}=-\frac{1}{\rho_0}\frac{\partial p}{\partial y}+\upsilon\left(\frac{\partial^2 v}{\partial x^2}+\frac{\partial^2 v}{\partial y^2}+\frac{\partial^2 v}{\partial z^2}\right)\\
&\frac{\partial w}{\partial t}+u\frac{\partial w}{\partial x}+v\frac{\partial w}{\partial y}+w\frac{\partial w}{\partial z}=-\frac{1}{\rho_0}\frac{\partial p}{\partial z}+\upsilon\left(\frac{\partial^2 w}{\partial x^2}+\frac{\partial^2 w}{\partial y^2}+\frac{\partial^2 w}{\partial z^2}\right)\\
&\frac{\partial T}{\partial t}+u\frac{\partial T}{\partial x}+v\frac{\partial T}{\partial y}+w\frac{\partial T}{\partial z}=0
\end{aligned}
\qquad (1)
$$

where ρ_0 is the constant density, u,v,w are the x-, y- and z- Cartesian coordinate system velocity components; *p* is the pressure, υ is the kinematic viscosity and *c* is the sound speed. We note that, for the sake of numerical efficiency with the current compressible flow solver, instead of the physical value for the sound speed in water an effective sound speed is used. The latter corresponds to a small subsonic Mach number $M_0=\sqrt{u^2+v^2+w^2}\,/\,c\approx 0.1-0.2,$ for which the compressibility effects on the turbulent eddies convected in the flow should be small. The apostoriori checks have confirmed that the numerical solution remains fairly insensitive to the Mach number variation within this range.

The external boundary conditions correspond to specifying the full velocity vector and temperature at the inlet boundaries and perscribing a constant static pressure at the outlet boundary. The inlet veloicty and temperarure conditions correspond to the fully developed turbulent fow before the junction in the main pipe (cold water) and the steady laminar boundary condition at the inlet of the long upper branch pipe (hot water). For the main pipe, the establishing of adeqaute numerical inflow conditions required a separate percurser pipe-flow simulation, from which the destribution of incoming velocity and tempertaure profiles have been extracted. For all solid walls, the no-slip condition is together with the zero temperature gradient normal to the wall, $\partial T/\partial n=0$.

2.2. Computational grid and solution algorithm

The solution domain for the T-junction problem spreads out for about 20 diameters both downstream of the junction and in the upstream part of the upper branch pipe and covered by a hexagonal cylindrical grid with a Cartesian block in the centre (Fig.2). No special grid generation effort has been dedicated to capturing the wall boundary layers on the pipe boundaries.

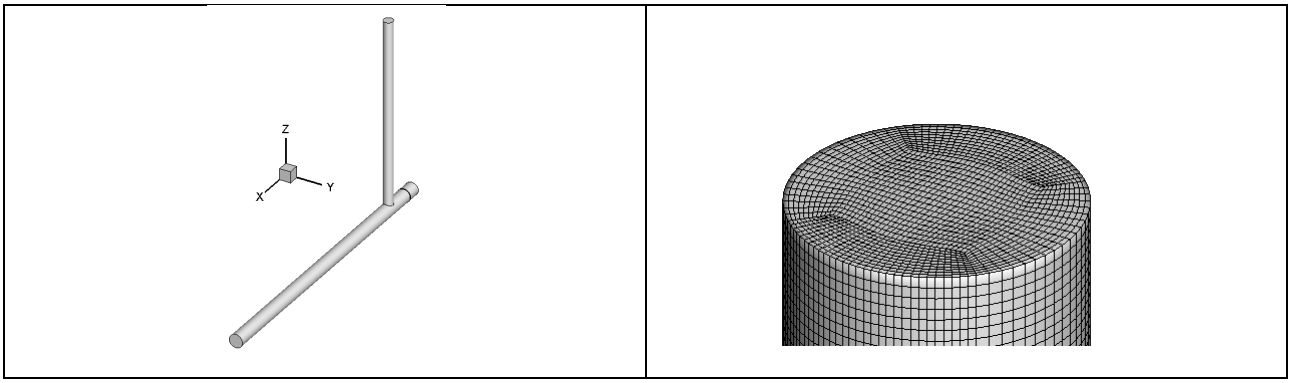

(a) (b)

Fig. 2 Computational grid for the T-junction configuration: full domain (a) and a zoomed-in view (b).

The CABARET algorithm is based on introducing conservation variables referred to the centres of the hexahedral elements and flux variables referred to the cell faces (fig.3).

At the conservation step the centre-cell variables are updated by summing up the fluxes over the faces belonging to the same cell:

$$
\begin{aligned}
u(t+\Delta t_{cell}) &= u(t)+\frac{\sum_{i=1}^{6}\left(p_i S_{xi}+\left(\upsilon\left(\frac{\Delta u}{\Delta x}\right)_i+u_i u_i\right)S_{xi}+\left(\upsilon\left(\frac{\Delta u}{\Delta y}\right)_i+u_i v_i\right)S_{yi}+\left(\upsilon\left(\frac{\Delta u}{\Delta z}\right)_i+u_i w_i\right)S_{zi}\right)}{V}\Delta t_{cell}\\
v(t+\Delta t_{cell}) &= v(t)+\frac{\sum_{i=1}^{6}\left(p_i S_{yi}+\left(\upsilon\left(\frac{\Delta v}{\Delta x}\right)_i+v_i u_i\right)S_{xi}+\left(\upsilon\left(\frac{\Delta v}{\Delta y}\right)_i+v_i v_i\right)S_{yi}+\left(\upsilon\left(\frac{\Delta v}{\Delta z}\right)_i+v_i w_i\right)S_{zi}\right)}{V}\Delta t_{cell}\\
w(t+\Delta t_{cell}) &= w(t)+\frac{\sum_{i=1}^{6}\left(p_i S_{zi}+\left(\upsilon\left(\frac{\Delta w}{\Delta x}\right)_i+w_i u_i\right)S_{xi}+\left(\upsilon\left(\frac{\Delta w}{\Delta y}\right)_i+w_i v_i\right)S_{yi}+\left(\upsilon\left(\frac{\Delta w}{\Delta z}\right)_i+w_i w_i\right)S_{zi}\right)}{V}\Delta t_{cell}\\
T(t+\Delta t_{cell}) &= T(t)-\frac{\sum_{i=1}^{6}T_i\left(u_i S_{xi}+v_i S_{yi}+w_i S_{zi}\right)}{V}\Delta t_{cell}\\
p(t+\Delta t_{cell}) &= p(t)-\rho_0 c^2\frac{\sum_{i=1}^{6}\left(u_i S_{xi}+v_i S_{yi}+w_i S_{zi}\right)}{V}\Delta t_{cell}
\end{aligned}
\qquad (2)
$$

where S_i, i=1,..,6 is the cell face normal and V is the cell volume. The gradients at the cell apex points are first obtained with the Gauss-Ostrogradsky theorem, e.g., for the x-velocity component:

$$
\frac{\Delta u}{\Delta x}=\frac{\sum_{j=1}^{J}S_{xj}\left(u_{bj}-u_{fj}\right)}{2\sum_{k=1}^{K}V_k},\quad \frac{\Delta u}{\Delta y}=\frac{\sum_{j=1}^{J}S_{yj}\left(u_{bj}-u_{fj}\right)}{2\sum_{k=1}^{K}V_k},\quad \frac{\Delta u}{\Delta z}=\frac{\sum_{j=1}^{J}S_{zj}\left(u_{bj}-u_{fj}\right)}{2\sum_{k=1}^{K}V_k}. \qquad (3)
$$

where J is the number of cell faces and K is the number of cell volumes that correspond to the given cell apex point, the index *b* stands for the current cell centre and the index *f* refers to the adjacent cell. Then the gradiants at the cell-face points are obtained by avearging the cell apex values.

For the cell side corresponding to the pipe wall boundary, the velocity difference $u_{bj}-u_{fj}$ is replaced by $2\beta u_{bj}$, where β is an adjustable numerical parameter that controls the amount of momentum transfer through the viscous wall: β=1 is used for well-resolved flow solution near the wall and the values 0.5<β<1 are used for coarse-grid simulations.

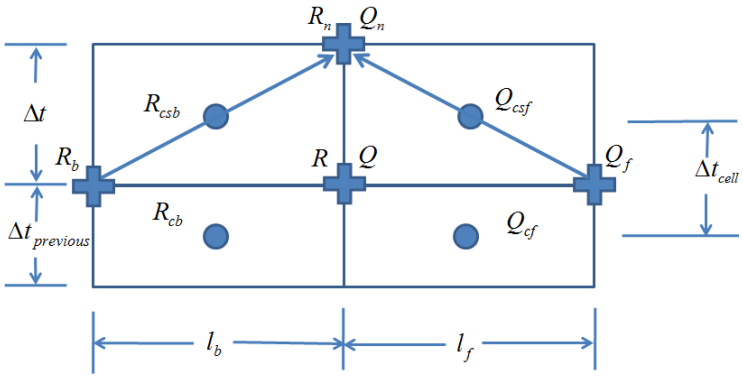

Fig. 3 Computational space-time stencil of the CABARET method

The conservation step is followed by the upwind extrapolation step. At this step the cell face values on the new time step are computed based on the characteristic decomposition. Here the one-dimensional Riemann variables are defined for each face normal projection

$$Q_{csf} = u_{scsf} - \frac{P_{csf}}{\rho_0 c}, R_{csb} = u_{scsb} + \frac{P_{csb}}{\rho_0 c}, u_{scsb} = \frac{u_{csb}S_x + v_{csb}S_y + w_{csb}S_z}{\sqrt{S_x^2 + S_y^2 + S_z^2}}. \quad (4)$$

The same decomposition is then performed for each cell-face and cell-centre points.

After this, the new values of the Riemann variables are then obtained by the second-order extrapolation

$$R_n = 2R_{csb} - R_b, Q_n = 2Q_{csf} - Q_f\ . \quad (5)$$

In accordance with the maximum principle, these values are truncated if found outside the allowable min and max values

$$\min\left(R, R_{cb}, R_b\right) + \left(\frac{R_{csb} - R_{cb}}{\Delta t_{cell}} + \left(u_{scsb} + c\right)\frac{R - R_b}{\Delta l_b}\right)\Delta t \le R_n \le \max\left(R, R_{cb}, R_b\right) + \left(\frac{R_{csb} - R_{cb}}{\Delta t_{cell}} + \left(u_{scsb} + c\right)\frac{R - R_b}{\Delta l_b}\right)\Delta t$$
$$\min\left(Q, Q_{cf}, Q_f\right) + \left(\frac{Q_{csf} - Q_{cf}}{\Delta t_{cell}} + \left(u_{scsf} - c\right)\frac{Q_f - Q}{\Delta l_f}\right)\Delta t \le Q_n \le \max\left(Q, Q_{cf}, Q_f\right) + \left(\frac{Q_{csf} - Q_{cf}}{\Delta t_{cell}} + \left(u_{scsf} - c\right)\frac{Q_f - Q}{\Delta l_f}\right)\Delta t \quad (6)$$

where $\Delta t_{cell} = \frac{\Delta t_{previous} + \Delta t}{2}, \Delta l = \frac{V}{\sqrt{S_x^2 + S_y^2 + S_z^2}}.$

For the inlet boundary, an inflow characteristic boundary condition is specified

$$P = \rho_0 c \frac{R_n - Q_{in}}{2}; u(x, y, z, t) = U_{in}(x, y, z, t); v(x, y, z, t) = V_{in}(x, y, z, t)$$
$$w(x, y, z, t) = W_{in}(x, y, z, t); T(x, y, z, t) = T_{in}(x, y, z, t) \quad (7)$$

For the main pipe, the inflow parameters $Q_{in}, U_{in}, V_{in}, W_{in}, T_{in}$ are obtained from a separate precurser calcuation in the single-periodic pipe domain. The parameters of the precurser calcuation were adjusted so that the average flow parameteres satisfied to the prescribed average flow quantities, e.g., the experimental flow rate.

For the main outlet, the outflow characteristic boundary condition is used together with a pressure relaxation condition for better numerical non-reflecting properties.

$$p_n = \alpha p_{out}(x, y, z, t) + \left(1 - \alpha\right) P_b, u_{\mathrm{n}} = R_{\mathrm{n}} - \frac{p_n}{\rho_0 c}. \quad (8)$$

The above numerical algorithm has been parallelised using MPI and METIS libraries and calculations have been conducted at the "SKIF" Supercomputing Facility of Moscow State University, HECToR UK Supercomputing Facility, and the HPC cluster at the Moscow Institute of Nuclear Safety. The computational grids used range from 2.10^5 to $14.3\ 10^6$ cells and the total number of time steps for the simulation has been from 100 000 to 1 000 000 time steps.

2.3. Numerical results

The CABARET solution sensitivity to the grid density has been first investigated by comparing the solutions obtained on several grids that correspond to 2.10^5, $1.8\ 10^6$ and $14.3\ 10^6$ grid cell volumes. The intermediate grid-range solution that corresponds to the grid of $1.8\ 10^6$ cells has been then submitted for the blind test competition. Instantaneous snapshots of the temperature field for all three grids are presented in Fig.5.

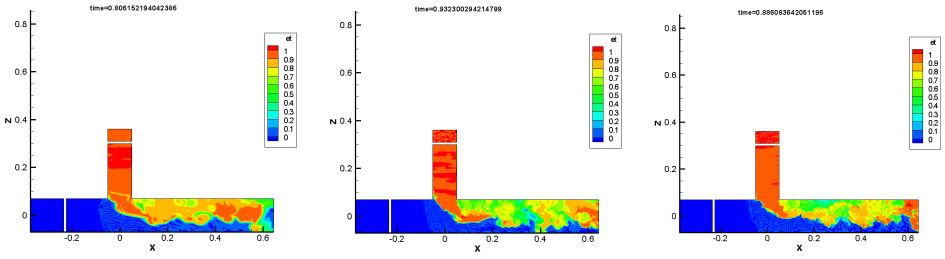

(a) (b) (c)

Fig. 5. Instantaneous snap shots of the temperature field in the T-junction domain symmetry plane (a reduced-size domain shown) for the grids of 2.10^5 (a), $1.8\ 10^6$ (b), and $14.3\ 10^6$ cells (c).

Not only the instantaneous velocity fields are found to only weakly depend on the grid resolution but also their simple time-means, r.m.s. (Fig.6a) and power-spectral density distributions (Fig.6b). With regard to the turbulent velocity spectra, it can also checked that more than one decade of the Kolmogorov -5/3 spectrum (straight black line) is captured with the CABARET code even on the moderate-size grid of $1.8\ 10^6$ cells.

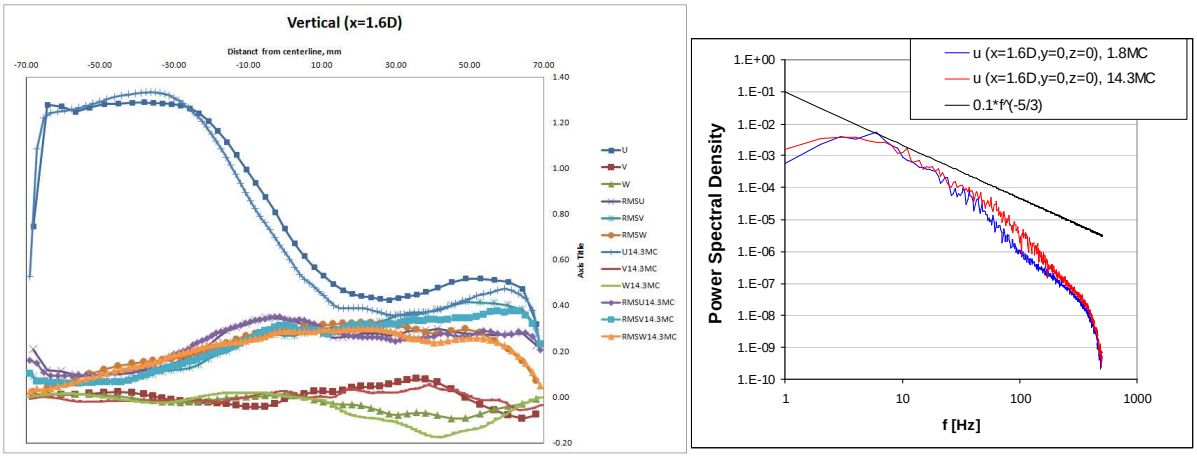

(a) (b)

Fig. 6. Grid resolution independence study for the CABARET ILES solution with 1.8 10^6 and 14.3 10^6 cells: time-averaged x-, y- and z-velocity components, U,V and W (U14.3MC,V14.3MC and W14.3MC for the 14.3 10^6 grid) and their r.m.s. fields in the symmetry plane at x=1.6D from the junction – (a) and the power spectral density of the x-velocity component at the pipe centre – (b).

Having checked the consistency of our LES solution we will now discuss how our results compare with the blind test data released. Figure 7 shows the axial temperature distribution (a) and its r.m.s. (b) at the sideline of the T-junction, the axial mean velocity and its r.m.s in the sideline and symmetry plane, as predicted from the CABARET ILES solution with 1.8 10^6 cells. The Vattenfall experiment data and the results of three fine-grid Fluent LES calculations (7 10^6, 34 10^6 and 70 10^6 cells) with a Smagorinsky subgridscale model are shown on the same plots for comparison. It can be seen that all three solutions are in an encouraging agreement with the experimental data. Note that the experimental error bars supplied with the current plots are shown for an illustration only and have to be treated with caution.

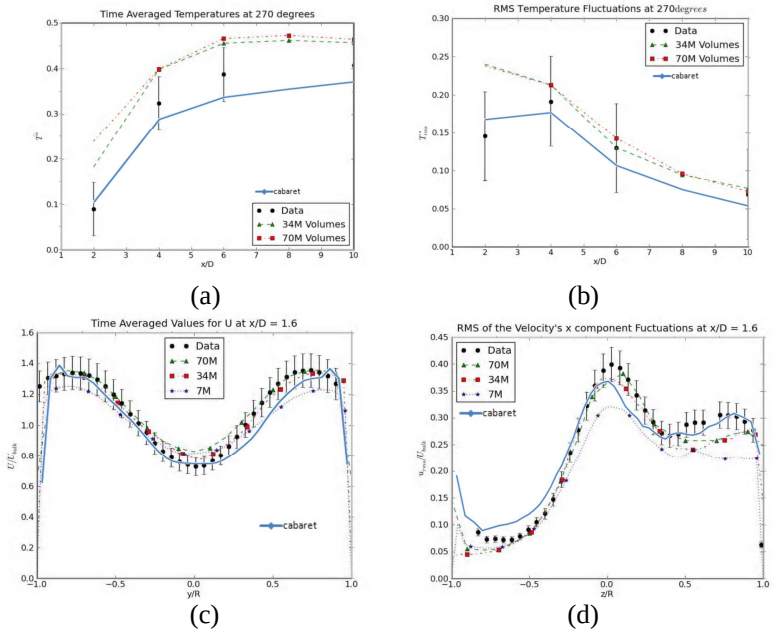

(a) (b)

(c) (d)

Fig. 7. Direct comparison with the released Vattenfall experiment and the first post-processed CFD (Fluent) data: temperature fields –(a),(b), axial velocity fields – (c),(d).

3. Conclusion

A novel Implicit LES CABARET method has been introduced and applied for the solution of the backward-facing step and the recent OECD/NEA-Vattenfall T-junction blind test exercise. In both cases the numerical solutions based on moderate grids are observed to be reasonably insensitive to the grid density and also correctly capturing the large-scale flow dynamics in comparison with the experiment and (for the T-junction test) with other fine-grid CFD results. For the T-junction problem, a reasonable solution convergence is also demonstrated for the r.m.s. and turbulence velocity power spectra. Most notably, more than one decade of the Kolmogorov -5/3rds spectrum is captured in all cases, which suggests that a wide range of important dynamic range of scales is correctly represented in the calculation.

References

[1] Iserles, A. "Generalized Leapfrog Methods", IMA Journal of Numerical Analysis, 6 (1986), No 3, pp 381-392.
[2] Goloviznin, V.M. "Balanced Characteristic Method for Systems of Hyperbolic Conservation Laws", Doklady Math., 72 (2005), pp619-623.
[3] Karabasov, S.A. and Goloviznin, V.M. "A New Efficient High-Resolution Method for Nonlinear Problems in Aeroacoustics", American Institute of Aeronautics and Astronautics Journal Vol. 45 (2007), pp2861-2871
[4] Goloviznin, V.M., Semenov, V.N., Korortkin, I.A and Karabasov, S.A. "A novel computational method for modelling stochastic advection in heterogeneous media", Transport in Porous Media, Springer Netherlands, 66(3) (2009), pp439-456.
[5] Karabasov, S.A. and Goloviznin, V.M. "Compact Accurately Boundary Adjusting high-REsolution Technique for Fluid Dynamics", Journal of Computational Physics, 228 (2009), pp7426–7451.
[6] Karabasov, S.A., Berloff, P.S., and Goloviznin, V.M., "CABARET in the Ocean Gyres", Journal of Ocean Modelling, 30 (2009), pp55–168.
[7] B. F. Armaly, F. Durtst, J. C. F. Pereira , and B. Schonung, "Experimental and theoretical investigation of backward-facing step flow", J . Fluid Mech. (1983), vol. 127, pp . 473-496.
[8] Westin, J., et al. (2008) High-cycle thermal fatigue in mixing Tees. Large-Eddy Simulations compared to a new validation experiment, ICONE16-48731, 16th International Conference on Nuclear Engineering, Orlando, Florida, USA, May 11-15, 2008.
[9] Angele, K., et al. (2009) High-cycle thermal fatigue in mixing Tees: New Large-Eddy Simulations validated against new data obtained by PIV in the Vattenfall experiment.
[10] Ridley, P. and Karabasov, S. "A Scalable Boundary Adjusting High-Resolution Technique For Turbulent Flows", Simulation Comes of Age CUG 2010 Conference, Edinburg, May 2010.